Two Novel Nitrogen-rich Metal-organic Nanotubes: Syntheses, Structures and Selective Adsorption toward Rare Earth

Minli Zhong[1], Siyao Xia[1], Sanmei Liu, Caiju Jin, Shengjun Deng*, Weiming Xiao, Shunmin Ding, Chao Chen*

Key laboratory of Jiangxi Province for Environment and Energy Catalysis, School of Chemistry and Chemical Engineering, Nanchang University, Nanchang, 330031, P. R. China

[1]*The first two authors contributed equally*

**To whom correspondence should be addressed. E-mail: Shengjun Deng: dshj1028@126.com; Chao Chen chaochen@ncu.edu.cn*

Contents

1 Experimental section

1.1 Characterization

The PXRD patterns for the samples were taken on a flat plate in the 2θ range 4-50°, using a Puxi DX-3 X-ray powder diffractometer, equipped with Cu Kα (λ = 1.5418 Å) radiation. The thermogravimetric analysis (TGA) was performed under a nitrogen atmosphere with the heating rate of 10 ℃ min^{-1} with METTLER TPLEDO DSC+ thermal analyzer. Fourier transform infrared (FT-IR) spectra of the samples were measured on a Agilent Cary 630 infrared spectrum apparatus using the KBr sheeting method in the range of 4000–400 cm^{-1}. The concentration of metal ions before and after adsorption were determined by Inductively Coupled Plasma Optical Emission Spectrometry (ICP-OES, Agilent, 5100). pH meter (INESA PHS-3C) was used to measure the pH of solutions and Zetasizer Nano series (Nano-ZS90) was used to measure the surface charge of the samples. The Perkin-Elmer 240 analyzer was applied to determine the contents of nitrogen, hydrogen and carbon. The Agilent Cary 60 spectrophotometer was applied to record the Ultraviolet–visible spectra. X-ray photoelectron spectroscopy (XPS) was conducted on a Thermo Scientific™ K-Alpha™+ spectrometer equipped with a monochromatic Al Kα X-ray source (1486.6 eV) operating at 100 W. Samples were analysed under vacuum (P < 10^{-8} mbar) with a pass energy of 150 eV (survey scans) or 50 eV (high-resolution scans). All peaks would be calibrated with C1s peak binding energy at 284.8 eV for adventitious carbon. Single-crystal diffraction data was collected on a CCD area detector diffractometer equipped with Mo K_α radiation (λ = 0.71073 Å). The structures were solved by direct methods and refined by full-matrix least-squares with Olex2 programs.[1] The disordered solvent molecules were removed by the SQUEEZE program.[2] CCDC 2206369 and 2206383 for NCD-166 and NCD-167 can be obtained free of charge from http://www.ccdc.cam.ac.uk/data_request/cif or by emailing data request@ccdc.cam.ac.uk, or by contacting The Cambridge Crystallographic Data Centre, 12 Union Road, Cambridge CB2 1EZ, UK; fax: +44 1223 336033.

1.2 Calculations of Adsorption Kinetics

The curves were fitted using pseudo-first-order model (Eq. S1), pseudo-second-order model (Eq. S2) and Weber-Morris intra-particle diffusion model (Eq. S3).

$$\ln(q_e - q_t) = \ln(q_t) - k_1 t \quad (1)$$

$$t/q_t = 1/(k_2 \times q_e^2) + t/q_e \quad (2)$$

$$q_t = kt^{0.5} + C \quad (3)$$

where q_e and q_t (mg g^{-1}) were the adsorption capacity at equilibrium and a specific time, respectively. k_1, k_2 (min^{-1})

and k (mg g^{-1} $min^{0.5}$) respectively represented the rate constant of pseudo-first-order model, pseudo-second-order model, and Weber-Morris models.

1.3 Calculations of Adsorption Isotherms

The adsorption isotherms were fitted using the Langmuir model (Eq. S4), and Freundlich model (Eq. S5)

$$C_e/q_e = 1/(K_L \times q_m) + C_e/q_m \quad (4)$$

$$\ln q_e = \ln K_F + (1/n) \ln C_e \quad (5)$$

1.4 Calculations of Selectivity Adsorption

The selectivity towards Eu^{3+} was determined through the calculation of the selectivity (S_{Eu}, %, Eq. S6).

$$S_{Eu} = \frac{q_{(Eu)}}{q_{(all\ ions)}} \times 100 \quad \ldots\ldots\ldots\ldots\ldots (7)$$

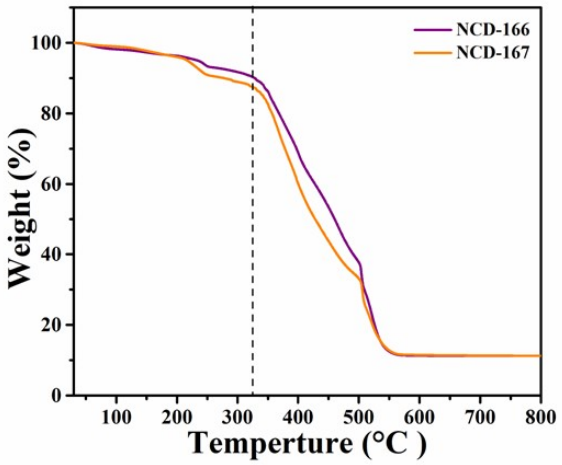

Fig. S1. TGA curves of **NCD-166** and **NCD-167**.

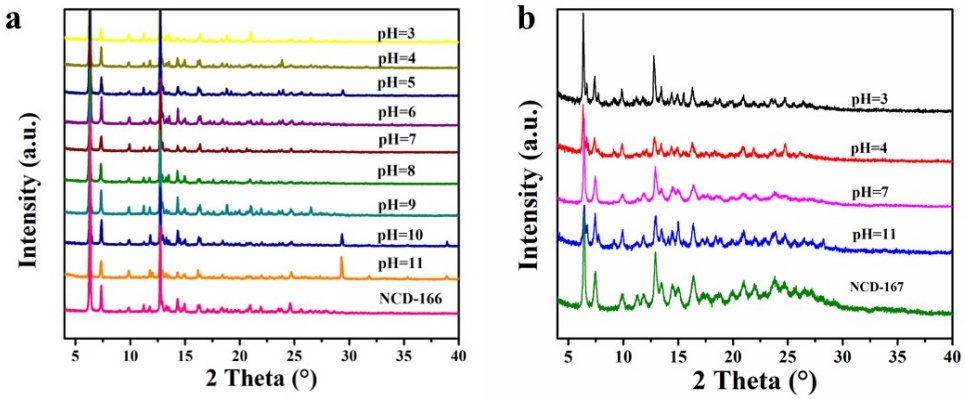

Fig. S2. PXRD patterns of **NCD-166** (a) and **NCD-167** (b) soaked in different pH aqueous solutions for 24 h.

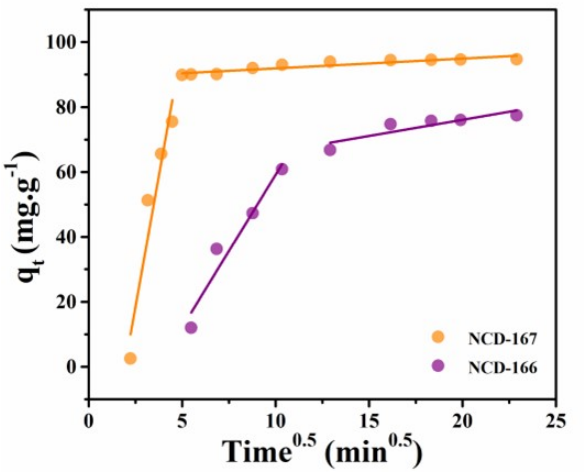

Fig. S3. The curves fitted by Weber-Morris intra-particle diffusion models for Eu^{3+} adsorption

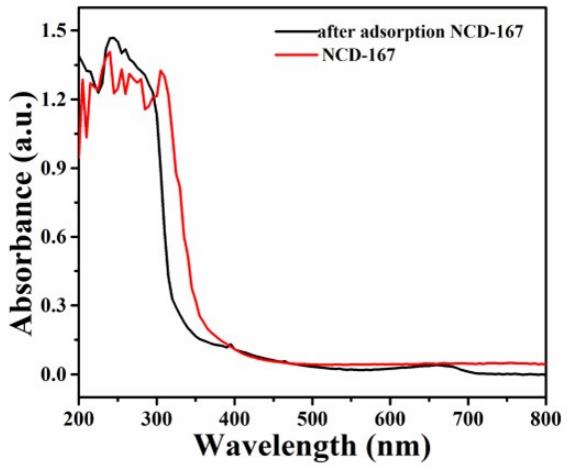

Fig. S4. Solid state UV-vis spectra of **NCD-167** before and after Eu^{3+} adsorption.

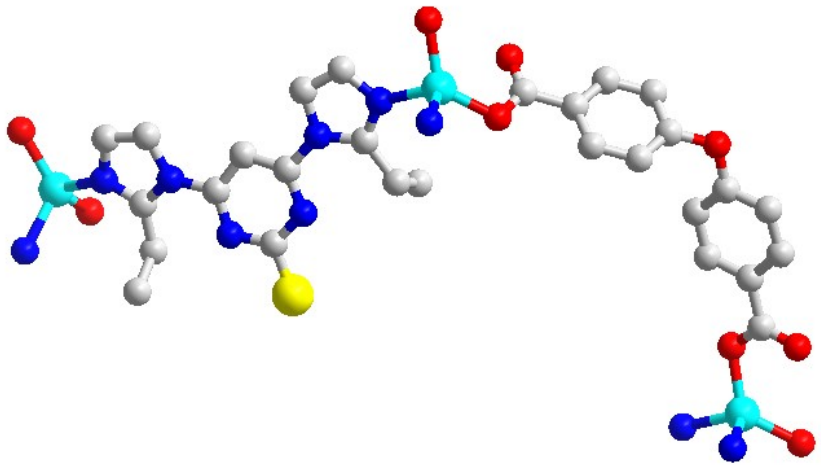

Fig. S5. The coordination environment of the organic ligands and Zn^{2+} ions of **NCD-167**.

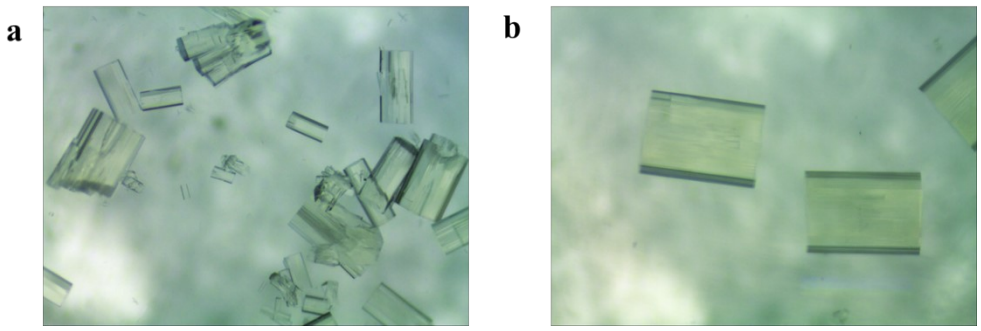

Fig. S6. Crystal photographs of **NCD-166** (a) and (b) **NCD-167**.

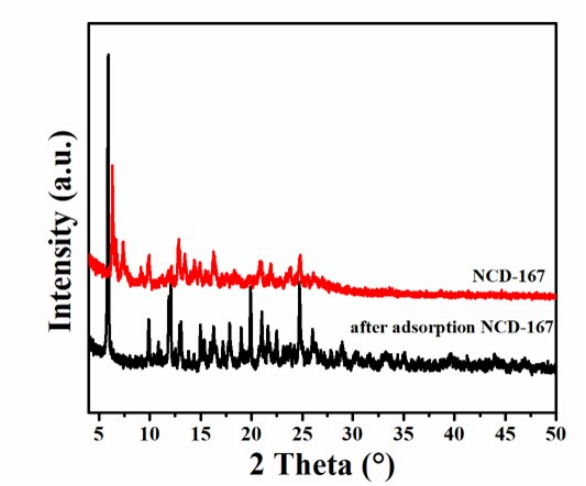

Fig. S7. PXRD pattern of **NCD-167** before and after Eu^{3+} adsorption.

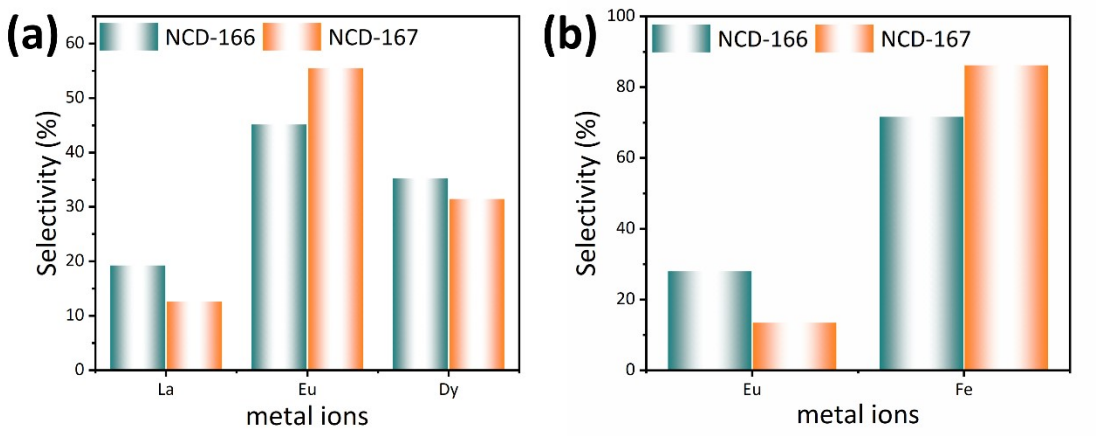

Fig. S8: (a) The recycling performance of **NCD-166** and **NCD-167**; (b) PXRD pattern of **NCD-166** and **NCD-167** before and after recycling.

Table S1. Crystal Data and Structure Refinement for **NCD-166** and **NCD-167**

Compound	NCD-166	NCD-167
Empirical formula	$C_{30}H_{26}N_6O_5Zn$	$C_{29}H_{26}N_6O_5Zn$

Formula weight	615.94	603.93
Temperature/K	100.15	100.15
Crystal system	trigonal	trigonal
Space group	P-3	P-3
a/Å	26.672(5)	26.7528(12)
b/Å	26.672(5)	26.7528(12)
c/Å	13.683(3)	13.4196(12)
α/°	90	90
β/°	90	90
γ/°	120	120
Volume/$Å^3$	8430(4)	8317.8(11)
Z	6	6
$\rho_{calc}g/cm^3$	0.728	0.723
μ/mm^{-1}	0.463	0.468
F(000)	1908	1872
Crystal size/mm^3	0.12 × 0.09 × 0.04	0.09 × 0.05 × 0.09
Radiation	MoKα (λ = 0.71073)	MoKα (λ = 0.71073)
2θ range for data collection/°	4.264 to 50.002	1.758 to 50.02
Index ranges	-31 ≤ h ≤ 31, -30 ≤ k ≤ 31, -14 ≤ l ≤ 16	-30 ≤ h ≤ 31, -27 ≤ k ≤ 31, -12 ≤ l ≤ 15
Reflections collected	41766	43031
Independent reflections	9930 [R_{int} = 0.1619, R_{sigma} = 0.1227]	9782 [R_{int} = 0.0834, R_{sigma} = 0.0755]
Data/restraints/parameters	9930/20/387	9782/14/378
Goodness-of-fit on F^2	1.053	1.041
Final R indexes [I>=2σ (I)]	R_1 = 0.0786, wR_2 = 0.2153	R_1 = 0.0567, wR_2 = 0.1775
Final R indexes [all data]	R_1 = 0.1325, wR_2 = 0.2725	R_1 = 0.0860, wR_2 = 0.2004
Largest diff. peak/hole / e $Å^{-3}$	0.95/-0.59	0.49/-0.39

Table S2. Comparison of adsorption capacity of different adsorbents for Eu^{3+}

	Material	Temperature (K)	pH	Adsorption Capacity (mg g^{-1})	Reference
Functionalized MOFs	UiO-66	298	4	43	3
	UiO-66-COOH	298	4	80	
	UiO-66-2COOH	298	4	150	
	Fe_3O_4 @ZIF-8	298	5	255.6	4
	Cr-MIL-PMIDA	298	5.5	85	5
	Cr-MIL-NH_2	298	5.5	12.5	
	UiO-66-CN	298		147.1	6
	UiO-66-AO	298		253.8	
	Co-MOF	298	5	52.93	7
	CMPO@MIL-101(Cr)	298	5	12.5	8
	UiO-66-NH_2 @ZIF-8	298	5	295.28	9
	Zn-BDC MOF/GO	298	4	39.01	24
Nanotubes	CMC/MMWCNTs	298	6	51	10
	Titanate nanotubes	298		18.8	11
	Humic acid-MWCNT hybrid	298	4.3	2.6	12
	Multiwall carbon nanotube	298	4.3	1.4	
	MWCNT/Fe_3O_4	298	4.5	9.1	13
	H-Titanates nanotubes short	298	4	22.8	14
	H-Titanates nanotubes long	298	4	9.8	
	TNTs	293	4.5	48.3	15
Biological composite	bio-PDA	298	6.5	151.52	16
Metal oxide	$[Me_2NH_2]$ V_3O_7			161.4	17
Molecular sieve	Molecular sieve (OMS-2)	298	5	106	18
Thiostannate	layered thiostannate			139	19
Ti_3C_2Tx MXene	Ti_3C_2Tx MXene (TCCH)	298	5	97.1	20
Graphene oxide (GO)	AO/mGO composites	293	4	69	21
	MnO_2/graphene oxide	298	5	83.5	22
	graphene oxide	298	5	68.4	
Clay	palygorskite	298	4	46.75	23
MONTs	**NCD-167**	**298**	**5**	**150.90**	**This work**

Table S3. The fitting results by the Weber-Morris intra-particle diffusion model of Eu^{3+} onto **NCD-167**

Material	Weber-Morris intra-particle diffusion model			
	$k_{Ⅰ}$ (mg g^{-1} $min^{0.5}$)	R^2	$k_{Ⅱ}$ (mg g^{-1} $min^{0.5}$)	R^2
NCD-166	9.41	0.92	0.99	0.72

NCD-167	32.30	0.89	0.30	0.85

References

1. O. V. Dolomanov, L. J. Bourhis, R. J. Gildea, J. A. K. Howard, and H. J. Puschmann, Appl. Crystallogr. 2009, 42, 339−341.

2. Spek, A. Acta Crystallogr. Section C **2015**, 71, 9−18.

3. Zhao, B.; Yuan, L.; Wang, Y.; Duan, T.; Shi, W. Carboxylated UiO-66 Tailored for U(VI) and Eu(III) Trapping: From Batch Adsorption to Dynamic Column Separation. *ACS Appl. Mater. Inter.* **2021,** 13 (14), 16300-16308.

4. Wu, Y.; Li, B.; Wang, X.; Yu, S.; Pang, H.; Liu, Y.; Liu, X.; Wang, X. Magnetic metal-organic frameworks (Fe_3O_4@ZIF-8) composites for U(VI) and Eu(III) elimination: simultaneously achieve favorable stability and functionality. *Chem. Eng. J.* **2019,** 378, 122105.

5. Sinha, S.; De, S.; Mishra, D.; Shekhar, S.; Agarwal, A.; Sahu, K. K. Phosphonomethyl iminodiacetic acid functionalized metal organic framework supported PAN composite beads for selective removal of La(III) from wastewater: Adsorptive performance and column separation studies. *J. Hazard. Mater.* **2022,** 425, 127802.

6. Wu, Y.; Li, B.; Wang, X.; Yu, S.; Liu, Y.; Pang, H.; Wang, H.; Chen, J.; Wang, X. Determination of practical application potential of highly stable UiO-66-AO in Eu(III) elimination investigated by macroscopic and spectroscopic techniques. *Chem. Eng. J.* **2019,** 365, 249-258.

7. Khalil, M.; Shehata, M. M.; Ghazy, O.; Waly, S. A.; Ali, Z. I. Synthesis, characterization and γ-rays irradiation of cobalt-based metal-organic framework for adsorption of Ce(III) and Eu(III) from aqueous solution. *Radiat. Phy. Chem.* **2022,** 190, 109811.

8. Fonseka, C.; Ryu, S.; Choo, Y.; Mullett, M.; Thiruvenkatachari, R.; Naidu, G.; Vigneswaran, S. Selective Recovery of Rare Earth Elements from Mine Ore by Cr-MIL Metal–Organic Frameworks. *ACS Sustainable Chem. Eng.* **2021,** 9 (50), 16896-16904

9. Zhang, M.; Yang, K.; Cui, J.; Yu, H.; Wang, Y.; Shan, W.; Lou, Z.; Xiong, Y. 3D-agaric like core-shell architecture UiO-66-NH_2@ZIF-8 with robust stability for highly efficient REEs recovery. *Chem. Eng. J.* **2020,** 386, 124023.

10. Zong, P.; Cao, D.; Cheng, Y.; Wang, S.; Hayat, T.; Alharbi, N. S.; Guo, Z.; Zhao, Y.; He, C. Enhanced performance for Eu(III) ion remediation using magnetic multiwalled carbon nanotubes functionalized with carboxymethyl cellulose nanoparticles synthesized by plasma technology. *Inorg. Chem. Front.* **2018,** 5 (12), 3184-3196.

11. Sheng, G.; Dong, H.; Shen, R.; Li, Y. Microscopic insights into the temperature-dependent adsorption of Eu(III) onto titanate nanotubes studied by FTIR, XPS, XAFS and batch technique. *Chem. Eng. J.* **2013,** 217, 486-494.

12. El-Sweify, F. H.; Abdelmonem, I. M.; El-Masry, A. M.; Siyam, T. E.; Abo-Zahra, S. F. Adsorption Behavior of Co(II) and Eu(III) on Polyacrylamide/Multiwalled Carbon Nanotube Composites. *Radiochemistry* **2019,** 61 (3), 323-330.

13. Chen, C. L.; Wang, X. K.; Nagatsu, M. Europium Adsorption on Multiwall Carbon Nanotube/Iron Oxide Magnetic Composite in the Presence of Polyacrylic Acid. *Environ. Sci. Technol.* **2009,** 43, 2362–2367.

14. Petrov, V.; Chen, Z.; Romanchuk, A.; Demina, V.; Tang, Y.; Kalmykov, S. Sorption of Eu (III) onto Nano-Sized H-Titanates of Different Structures. *Appl. Sci.* **2019,** 9 (4), 697.

15. Lu, S.; Ma, B.; Wu, S.; Zhou, J.; Wang, X. Comparison sorption properties of Eu(III) on titanate nanotubes and rutile studied by batch technique. *J. Radioanal. Nucl. Chem.* **2015,** 306 (2), 527-534.

16. Zhou, X.; Liu, W.; Tian, C.; Mo, S.; Liu, X.; Deng, H.; Lin, Z. Mussel-inspired functionalization of biological calcium carbonate for improving Eu(III) adsorption and the related mechanisms. *Chem. Eng. J.* **2018,** 351, 816-824.

17. Sun, H.; Liu, Y.; Lin, J.; Yue, Z.; Li, W.; Jin, J.; Sun, Q.; Ai, Y.; Feng, M.; Huang, X. Highly Selective Recovery of Lanthanides by Using a Layered Vanadate with Acid and Radiation Resistance. *Angew. Chem. Int. Ed.* **2020,** 59 (5),

1878-1883.

18. Yin, L.; Hu, B.; Zhuang, L.; Fu, D.; Li, J.; Hayat, T.; Alsaedi, A.; Wang, X. Synthesis of flexible cross-linked cryptomelane-type manganese oxide nanowire membranes and their application for U(VI) and Eu(III) elimination from solutions. *Chem. Eng. J.* **2020,** 381, 122744.

19. Qi, X. H.; Du, K. Z.; Feng, M. L.; Gao, Y. J.; Huang, X. Y.; Kanatzidis, M. G. Layered $A_2Sn_3S_7.1.25H_2O$ (A = Organic Cation) as Efficient Ion-Exchanger for Rare Earth Element Recovery. *J. Am. Chem. Soc.* **2017,** 139 (12), 4314-4317.

20. Zhang, P.; Wang, L.; Du, K.; Wang, S.; Huang, Z.; Yuan, L.; Li, Z.; Wang, H.; Zheng, L.; Chai, Z.; Shi, W. Effective removal of U(VI) and Eu(III) by carboxyl functionalized MXene nanosheets. *J. Hazard. Mater.* **2020,** 396, 122731.

21. Hu, B.; Guo, X.; Zheng, C.; Song, G.; Chen, D.; Zhu, Y.; Song, X.; Sun, Y. Plasma-enhanced amidoxime/magnetic graphene oxide for efficient enrichment of U(VI) investigated by EXAFS and modeling techniques. *Chem. Eng. J.* **2019,** 357, 66-74.

22. Ma, J.; Zhao, Q.; Zhou, L.; Wen, T.; Wang, J. Mutual effects of U(VI) and Eu(III) immobilization on interpenetrating 3-dimensional MnO_2/graphene oxide composites. *Sci. Total Environ.* **2019,** 695, 133696.

23. Zhu, Y.; Chen, T.; Liu, H.; Xu, B.; Xie, J. Kinetics and thermodynamics of Eu(III) and U(VI) adsorption onto palygorskite. *J. Mol. Liq.* **2016,** 219, 272-278.

24. Chen, Z.; Li, Z.; Chen, J.; Tan, H.; Wu, J.; Qiu, H. Selective Adsorption of Rare Earth Elements by Zn-BDC MOF/Graphene Oxide Nanocomposites Synthesized via In Situ Interlayer-Confined Strategy. *Ind. Eng. Chem. Res.* **2022,** 61 (4), 1841-1849.